FULL RESEARCH ARTICLE

Mechanical properties of laser powder bed fusion produced overhang parts with different support geometries: an experimental study

Orhan Gülcan[1] · Kadir Günaydın[1] · Alican Çelik[1] · Evren Yasa[2]

Abstract

Additive manufacturing technologies give engineers and researchers a high level of design freedom to produce complex components or entire assemblies previously impossible or impractical to manufacture by conventional means. Although additive manufacturing has many advantages compared to conventional machining, it has some drawbacks, two of which are higher surface roughness and dimensional inaccuracy of as-built part surfaces especially in overhang features. Support structures are one of the solutions to mitigate these drawbacks at a cost of additional post-processing efforts. The aim of the present study is to investigate the effect of different support geometries on the mechanical properties of laser powder bed fusion manufactured Inconel 718 overhang parts. The tested support geometries are comprised of several pieces to ease post-processing instead of using single-piece supports filling all over the overhang surface. One of the tested support structures is contactless support with no direct contact between the part and the support itself. The others are tooth support where the contact is on the tooth faces and line support where the contact is along a line. The thickness of each support piece and the spacing between the two support pieces were used as design variables. The dimensional accuracy of printed specimens with respect to the computer-aided geometry, distortion of overhang features, microhardness through the thickness, microstructural changes of overhang surface, and surface roughness of overhang features was experimentally evaluated. The results revealed that support type, support spacing and support thickness directly affect the performance characteristics used in this study.

Keywords Laser powder bed fusion · Contactless support · Tooth support · Line support · Downskin surfaces

1 Introduction

Considered as one of the pillars of the fourth industrial revolution [1], Additive Manufacturing (AM) or three-dimensional (3D) printing is a layer-by-layer manufacturing process in which a part can be built on a build plate from a 3D computer-aided design (CAD) file sliced in a virtual environment, and then for each slice a machine-specific tool path is generated [2]. Unlike conventional methods, namely subtractive manufacturing methods, AM is based on incremental layer-by-layer manufacturing [3]. AM gives engineers and researchers new design freedom to produce enhanced components or entire assemblies which were

previously impossible or impractical to manufacture [4]. In Powder Bed Fusion (PBF) processes, a group of AM processes, powder particles are laid on the build plate attached to the build platform by a recoater blade. For each layer, generally a laser or electron beam is used to selectively melt the powder particles layer by layer. According to the employed energy source, the process is called the laser powder bed fusion (LPBF) or electron beam powder bed fusion (EPBF) process. Although PBF processes have many advantages compared to conventional machining, they have still some bottlenecks to be overcome. The most important disadvantages limiting the adoption of these processes are mainly insufficient surface roughness and dimensional inaccuracy in comparison to conventional manufacturing methods [5].

In most of the studies related to the metal PBF processes, the bad surface quality is mainly attributed to the stair-step effect due to the inherent nature of AM processing and partially melted powders bonded to the surface [6]. Especially when materials with high thermal conductivity such as copper or aluminum are used, a deeper heat-affected zone is

✉ Orhan Gülcan
  orhan.gulcan@ge.com

1 General Electric Aviation, Additive Design, Kocaeli, Turkey

2 Mechanical Engineering Department, Eskişehir Osmangazi University, Eskişehir, Turkey

formed on the surface, which leads to more powder adhering to the surface without fully melting and consequently higher surface roughness [7]. In general, downskin surfaces, also called as overhang surfaces, have higher surface roughness than other surfaces, i.e., upskin or vertical surfaces, due to the fact that heat transfer phenomena through angled surfaces result in bigger overheating zones in downskin surfaces which eventually causes more particle adhesion [8]. High surface roughness of as-built samples was also attributed to surface pores due to the lack of fusion and adhesion of partially melted powder particles [9]. Partially melted powder particles increase the surface roughness of printed part surfaces. These rough surfaces play a very important role in stress–strain behavior of AM parts especially in small cross-sectional areas [10]. Moreover, the high surface roughness of as-built samples gives rise to reduced corrosion resistance when compared to polished samples having higher surface quality [11]. As expected, the surface roughness also affects the fatigue life of AM parts [12]. It is found in the literature that the surface roughness of built parts is more influential in high cycle fatigue (HCF) rather than low cycle fatigue (LCF) applications [13]. Jamshidinia et al. compared fatigue behaviors of Ti6Al4V lattice structures produced by the EPBF process revealing that high surface roughness, low strut thickness and low relative density have the highest impact on fatigue life and the crack initiation was mostly started in strut surfaces where partially melted powder particles attached to [14]. Vayssette et al. investigated the effect of surface roughness of Ti6Al4V parts produced by LPBF and EPBF processes and reported a significant decrease in the HCF life of as-built parts due to higher surface roughness compared to machined parts [15, 16].

To enable manufacturability in LPBF, the support structure is one of the main elements. As a general rule of thumb, if a part surface has an inclination below 45° with respect to the build plate, it needs to be supported. Above this angle, the surfaces are self-supporting, thus no need fo extra support structures [17]. The design and location of support structures are also important for the resulting surface quality and dimensional accuracy. Inappropriate support designs may result in higher surface roughness and even build failures when these structures are physically removed after

manufacturing [18]. Leary also stated the importance of the remnants of the support structures on the surface roughness since the mechanical removal of these structures after the build process may result in surface irregularities and/or distortions at mating locations [19]. For especially overhanging sections, support structures withstand material fall-in and part warpage due to thermal gradients by thermal-induced stresses [20].

Different support geometries used on overhang features have different thermal conductivities, therefore, their effects on surface roughness and dimensional accuracy are also different [21]. For this reason, different types of support have been investigated in the literature as shown in Fig. 1 [22]. Järvinen et al.'s study revealed that web support showed better surface quality parts than tube supports [22]. Umer et al. investigated the deformation behavior of overhang features with column and Y-shape supports produced by EPBF and stated nearly 22% deviations between experimental and simulation results due to the deviations in material properties, deformation in build plate and assumption of no deformation in lateral direction [23]. In terms of contactless supports where there is no direct contact between the part and the support, 0.49 mm, 0.63 mm, 0.77 mm [24], 0.3, 0.45, 0.75 mm [18] and 0.21 mm [25, 26] gaps were used between the part and the support, and it was revealed that when the gap distance is decreased, the deformation of the overhang surfaces decreased. In terms of tooth supports, it was stated in the literature that z-height, defined as the offset between the top of tooth support and the mating surface of parts, has a considerable effect on part deformation for LPBF overhang parts [27]. In another study, it was stated that z-height affects the part deformation for Ti6Al4V parts, but it has no considerable effect on AlSi10Mg parts produced by LPBF [28]. In Ameen et al.'s studies, it was shown that tooth supports can be located 2–5 mm away from the beginning of the overhang section without having any significant effect on deformation [29, 30].

In nearly all the studies carried out in the literature about the effect of support types on the mechanical properties of overhang parts produced by PBF processes, full single-piece supports under overhang surfaces were used. However, supports composed of multiple pieces can be used under
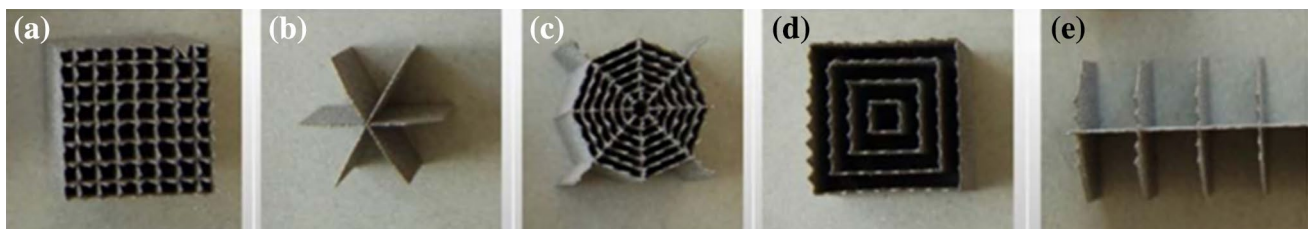

Fig. 1 Different types of supports used in literature: **a** block, **b** point, **c** web, **d** contour, **e** line support [22]

overhang surfaces rather than a single piece to reduce the amount of powder used and time spent for printing as well as to ease the post-processing. Kurzynowski et al. stated that columnar pores formation and mechanical properties of the final part are directly influenced by the distance between support pieces and their inclination with respect to the build plate when multiple support pieces are used under overhang features [31]. To the best of authors' knowledge, no study has so far focused on using a different type of supports with multiple pieces and their effects on the mechanical properties of the final part. To fill this gap in the literature, the present study focused on three types of supports: contactless support, tooth support and line support. Supports with multiple pieces and overhang specimens were produced from Inconel 718 material by the LPBF process. Apart from support types, the thickness of each support piece and the spacing between two support pieces were also used as design variables. Dimensional accuracy of printed specimens with respect to CAD geometry, distortion of overhang feature, microhardness through the thickness, microstructural changes of overhang surface, and surface roughness of overhang features were experimentally measured. The rest of the paper is organized as follows: different support design, manufacturing and measurement techniques are detailed in Sect. 2. Results in terms of average thickness deviation, surface roughness, microhardness through thickness and microstructure are discussed in Sect. 3 and lastly key findings in this study is summarized in the Conclusion section.

2 Materials and methods

The specimen geometry with an overhang surface of 30° used in this study is shown in Fig. 2. 3D geometries of the specimen and supports were modelled using Siemens NX 12 software (Siemens AG, Germany). As shown in Figs. 3, 4 and 5, three different types of supports were used in the study: contactless support where there is no direct contact between the part and the support, tooth support where the contact is on the tooth faces and line support where the contact is along a line. Instead of using single-piece support filling all over the overhang surface, different types of supports composed of multiple pieces were used. The thickness of each support pieces (dimension A in Figs. 3, 4 and 5) and the spacing between two support pieces (dimension B in Figs. 3, 4 and 5) were used as design variables. A full set of designs of experiments was used in this study with three factors at three levels. Table 1 shows the related data for the total 27 experiments.

The specimens were located on the build plate as shown in Fig. 6. For each configuration of 3 factors, three specimens, in other words repetitions, and a total of 81 specimens were produced in two builds.
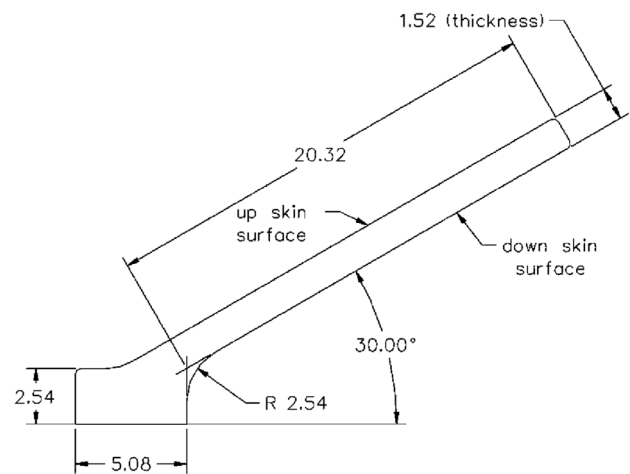

Fig. 2 General dimensions of overhang specimen (dimensions are in mm, width: 25.4 mm)

The specimens were manufactured using a Concept Laser M2 direct laser melting (DMLM) machine, a commercial name for LPBF, (Concept Laser GmbH, GE Additive, Germany) from Inconel 718 material. DMLM manufacturing was performed under a nitrogen gas environment and 50 μm layer thickness was used. The chemical composition of the Inconel 718 material used in production is shown in Table 2, and the standard vendor process parameters were used during manufacturing as presented in Table 3.

Solukon SFM-AT800 system (Solukon Maschinenbau GmbH, Augsburg, Germany) was used for the powder evacuation process after the DMLM build. After the powder evacuation process, specimens and supports were removed from the build plate with the help of the GF AgieCharmilles wire electrical discharge machine (Agie Charmilles Ltd., Switzerland) with a wire thickness of 0.3 mm and an average cutting speed of 5 mm/min. After removing from the build plate, support structures were removed from the specimens manually.

For dimensional deviation and distortion measurements, ATOS ScanBox 4105 blue light device (Carl Zeiss GOM Metrology GmbH, Braunschweig, Germany) was used. Scanned manufactured specimens were compared with the original CAD geometry by using GOM Inspect software (Carl Zeiss GOM Metrology GmbH, Braunschweig, Germany). Alicona InfiniteFocus G5 (Alicona Imaging GmbH, Graz, Austria) based on the focus variation technique was used for surface roughness measurements. During surface roughness (S_a) measurements, X10 magnification, polarized coaxial illumination, 6 μm lateral resolution and 900 nm vertical resolution were used. The specimens were cut from its middle plane with a Struers Secotom cutter, mounted in Struers CitoPress mounting machine and finally polished with Struers Tegramin (Struers LLC, Ohia,
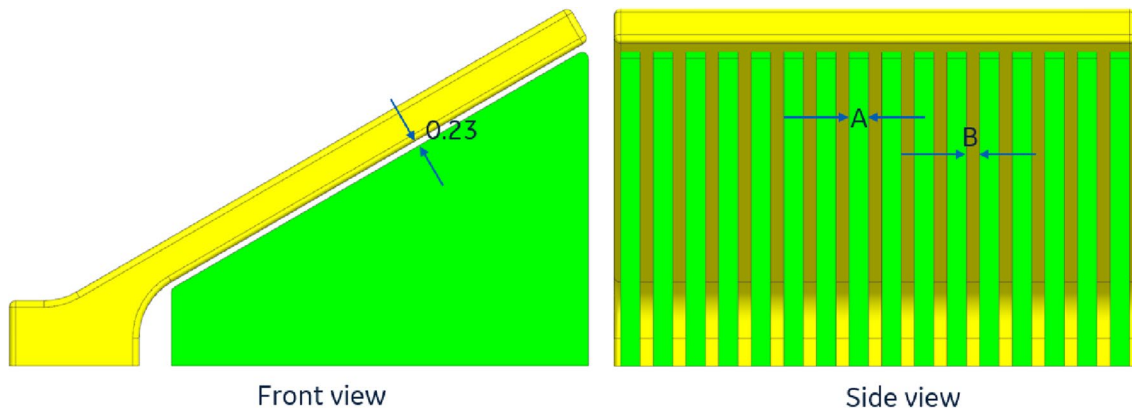
Fig. 3 Contactless support (dimensions are in mm). See Table 1 for A and B
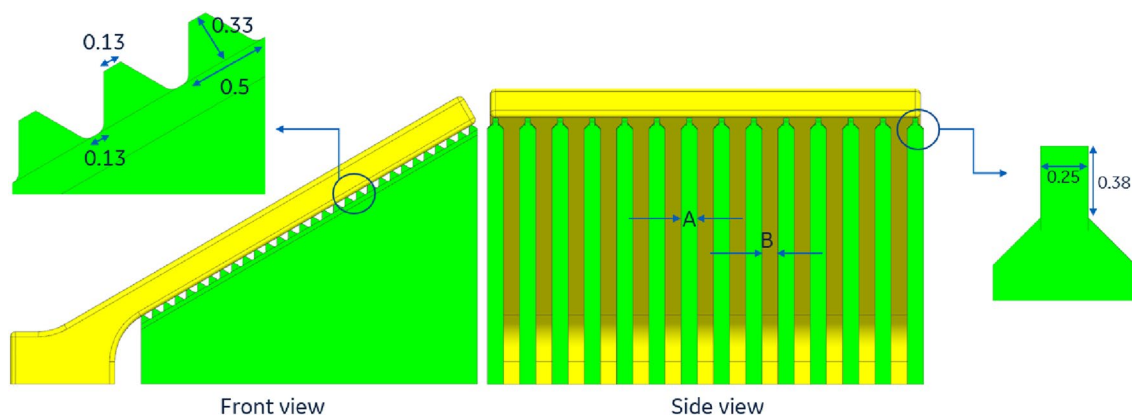

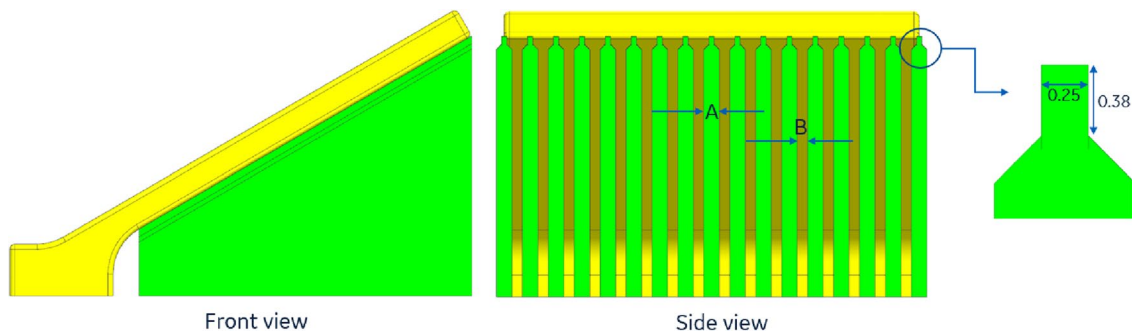**Fig. 4** Tooth support (dimensions are in mm). See Table 1 for A and B

Fig. 5 Line support (dimensions are in mm). See Table 1 for A and B

US) for metallographic studies and microhardness measurements. For metallographic studies, Nikon Eclipse MA200 optical microscope (Nikon corp., Tokyo, Japan) and Zeiss Merlin FE-SEM scanning electron microscope (Carl Zeiss AG, Jena, Germany) were used. Emco-Test DuraScan-70 type micro hardness tester equipment (EMCO-TEST Prüf-maschinen GmbH, Kuchl, Austria) at Vickers hardness scale 0.3 (HV 0.3, 2.942 N) was used for hardness measurements. Microhardness through thickness evaluations were performed by measuring three microhardness values at the near upper edge, at the middle and at the near lower edge. For all measurements, three specimens for each experiment set were measured and the average values were used in the evaluations.

Table 1 Design of experiment (dimensions are in mm)

Experiment no.	Support type	Dimension A	Dimension B
1	Contactless	0.76	0.51
2	Contactless	0.76	0.76
3	Contactless	0.76	1.02
4	Contactless	1.02	0.51
5	Contactless	1.02	0.76
6	Contactless	1.02	1.02
7	Contactless	1.27	0.51
8	Contactless	1.27	0.76
9	Contactless	1.27	1.02
10	Line	0.76	0.51
11	Line	0.76	0.76
12	Line	0.76	1.02
13	Line	1.02	0.51
14	Line	1.02	0.76
15	Line	1.02	1.02
16	Line	1.27	0.51
17	Line	1.27	0.76
18	Line	1.27	1.02
19	Tooth	0.76	0.51
20	Tooth	0.76	0.76
21	Tooth	0.76	1.02
22	Tooth	1.02	0.51
23	Tooth	1.02	0.76
24	Tooth	1.02	1.02
25	Tooth	1.27	0.51
26	Tooth	1.27	0.76
27	Tooth	1.27	1.02
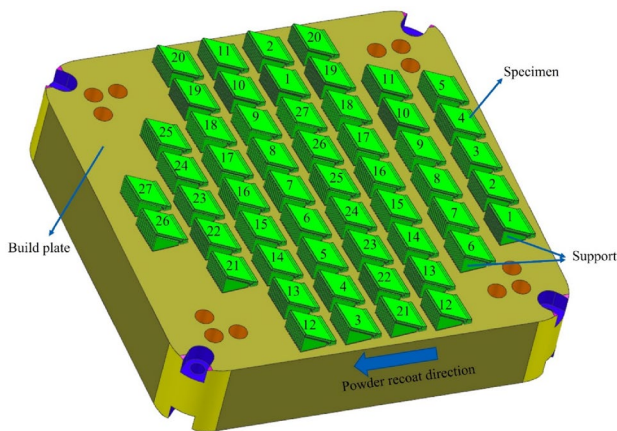
Fig. 6 Specimen layout on build plate. Numbers show the specimen no

The importance of each design variable on design outputs and the optimum parameter sets to obtain the optimum design outputs were found by using analysis of variance (ANOVA). Minitab 19 software was used for ANOVA analysis.

3 Results and discussions

All specimens were successfully produced without any manufacturability issues as depicted in Figs. 7 and 8.

3.1 Average thickness deviation and distortion results

Average thickness deviation measurements were performed on 6 locations for each specimen as shown in Fig. 9. Measured average thickness deviations are shown in Fig. 10 in terms of support thickness and support spacing for three different types of supports.

From Fig. 10, it is pretty clear that, for contactless supports, the minimum (0.0073 mm) and maximum (0.1063 mm) average thickness deviations were observed at 0.51 mm support spacing with 0.76 mm support thickness and 1.02 mm support spacing with 1.02 mm support thickness, respectively. Support spacing increase resulted in an increase in average thickness deviation for all support thickness values. This is probably due to the fact that when support spacing increases, more freestanding melt pools penetrate towards the loose powder bed, more powders stick to the melt pool and increases the surface roughness and deviations [33–36]. For the fixed support spacing, average thickness deviation increased when the support thickness increased, except for the 1.02 mm support spacing. When the spacing between supports increased from 0.51 mm to 0.76 mm and from 0.76 mm to 1.02 mm, average thickness deviation increased nearly 134% and 41%, respectively, for 0.76 mm support thickness, 131% and 44%, respectively, for 1.02 mm support thickness and 16% and 2%, respectively, for 1.27 mm support thickness. From these percentage calculations, it can be concluded that for contactless supports, the percentage of increase in thickness deviation related to an increase in support spacing is lower for thicker supports.

For line supports, the minimum (0.0423 mm) and maximum (0.5897 mm) average thickness deviations were observed at 0.51 mm support spacing with 1.27 mm support thickness and 1.02 mm support spacing with 0.76 mm support thickness, respectively. Similar to the contactless supports, the support spacing increase resulted an increase in average thickness deviation for all support thickness values. There is no direct correlation found between support thickness and average thickness deviation. When the spacing between supports increased from 0.51 mm to 0.76 mm and from 0.76 mm to 1.02 mm, average thickness deviation increased nearly 41% and 67.5%, respectively, for 0.76 mm

Table 2 Chemical composition of Inconel 718 wt%

Element	Ni	Cr	Nb	Mo	Ti	Mn	Si	Al	Fe
wt %	53.00	18.50	5.00	3.00	0.66	3.00	0.35	0.35	Balance

Table 3 Processing parameters [32]

	Laser power (W)	Laser scan speed (mm s^{-1})	Laser spot size (μm)
Skin	160	800	80
Core	160	680	53

support thickness, 47% and 10%, respectively, for 1.02 mm support thickness and 149% and 38%, respectively, for 1.27 mm support thickness.

For tooth supports, the minimum (0.1338 mm) and maximum (0.2611 mm) average thickness deviations were observed at 0.51 mm support spacing with 0.76 mm support thickness and 1.02 mm support spacing with 1.27 mm
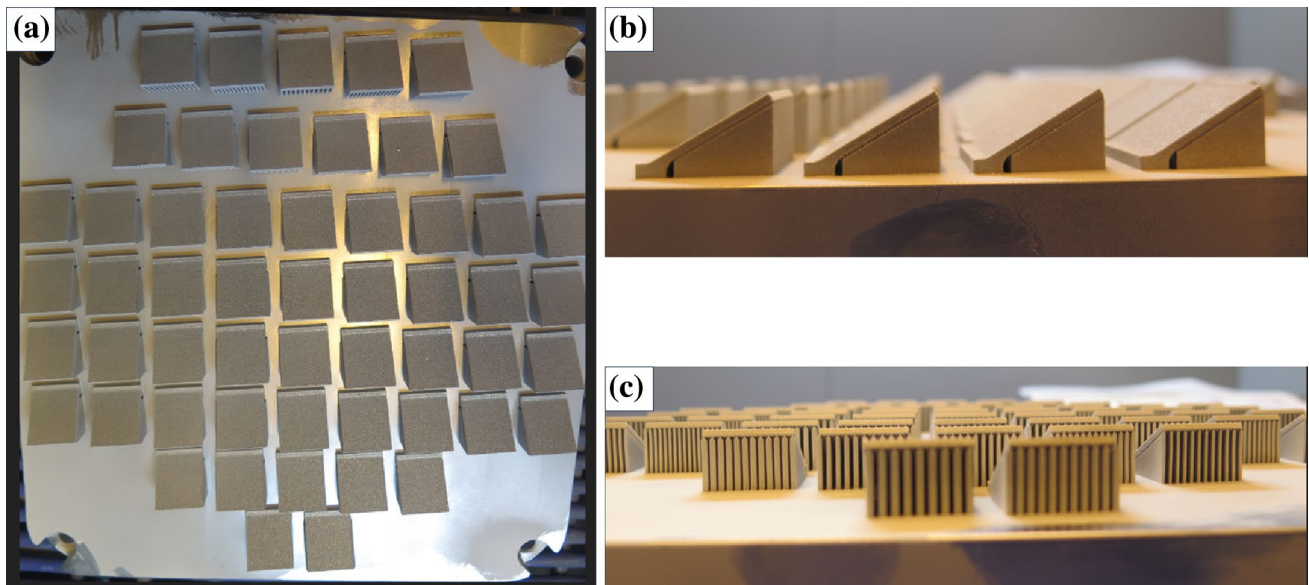
Fig. 7 Produced specimens after powder removal: **a** top view, **b** side view, **c** front view
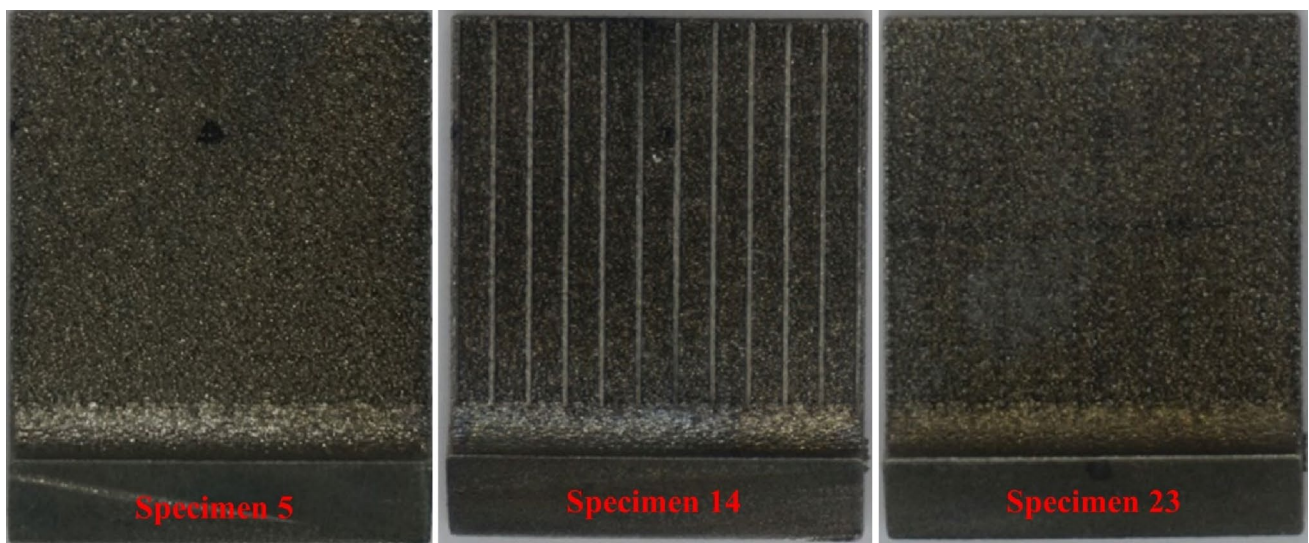
Fig. 8 Downskin surfaces of three specimens related with three different support types after wire EDM cut
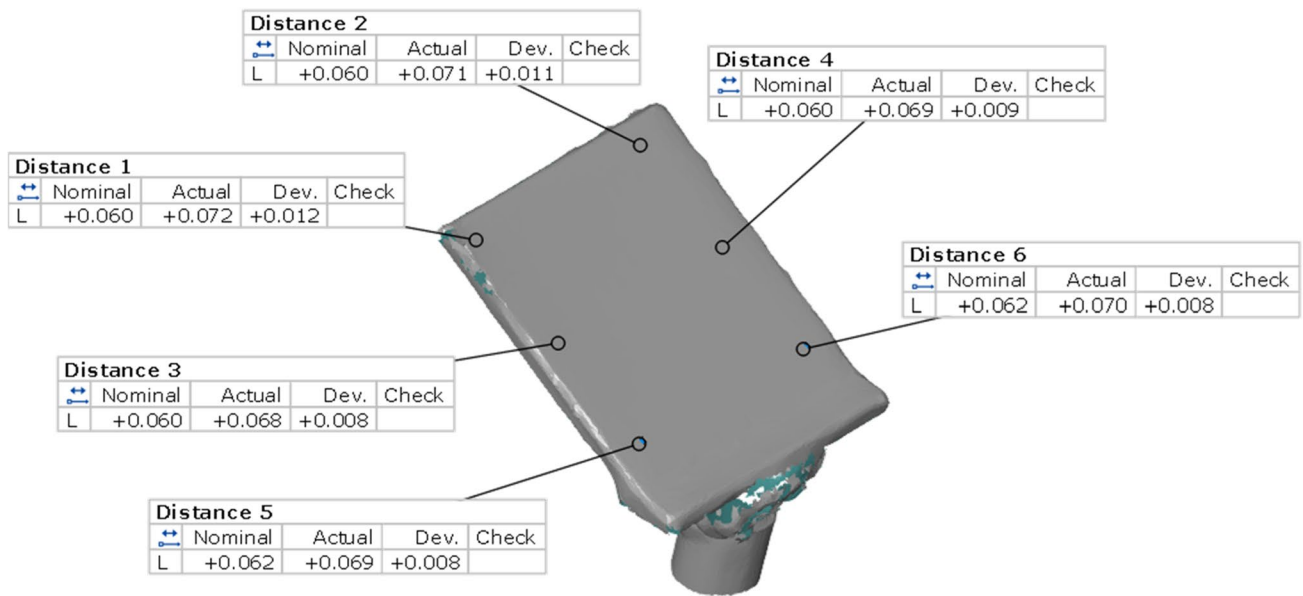
Fig. 9 Thickness deviation measurements from 6 locations
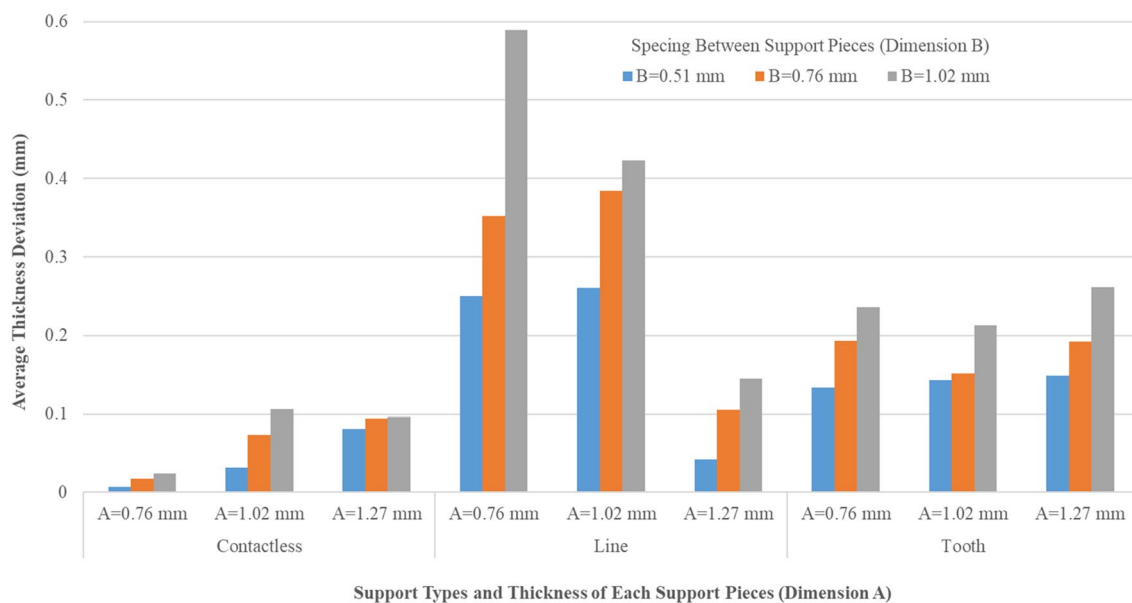

Fig. 10 Average thickness deviations for all specimens

support thickness, respectively. There is a direct correlation between support spacing and average thickness deviation for all support thickness values. However, similar to the line support, there is no direct correlation found between support thickness and average thickness deviation. When the spacing between supports increased from 0.51 mm to 0.76 mm and from 0.76 mm to 1.02 mm, average thickness deviation increased nearly 44% and 22%, respectively, for 0.76 mm support thickness, 6% and 40.5%, respectively, for

1.02 mm support thickness and 29% and 36%, respectively, for 1.27 mm support thickness.

For the investigated three different types of support structures, the minimum and maximum average thickness deviation were observed at the smallest (0.51 mm) and at the highest (1.02 mm) support spacings.

Main effect plot from ANOVA analysis of average thickness deviation is shown in Fig. 11. Since lower average thickness deviation means higher performance, it can
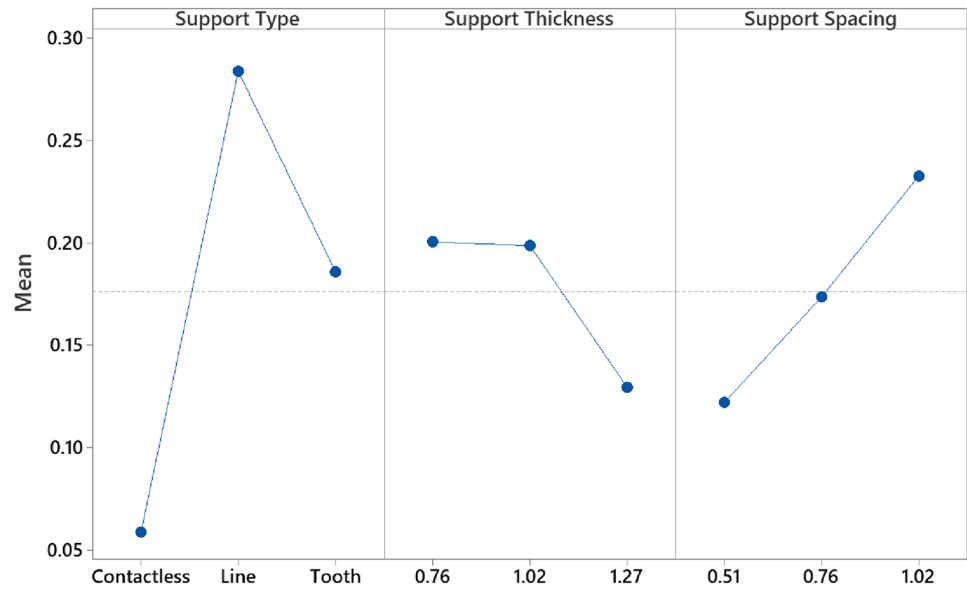
Fig. 11 Main effect plot for average thickness deviation

Table 4 ANOVA for average thickness deviation

Source	DF	Adj SS	Adj MS	F value	p value
Support type	2	0.22847	0.114233	12.55	0.0003
Support thickness	2	0.02941	0.014705	1.62	0.2237
Support spacing	2	0.05509	0.027544	3.03	0.0711
Error	20	0.18205	0.009102		
Total	26				

be concluded from Fig. 11 that contactless support with 1.27 mm support thickness and 0.51 mm support spacing is the optimum parameter set for the lowest average thickness deviation in the scope of the experimental set used in this study. It was also observed in the literature that dimensional accuracy for contactless supported specimens is related to not only support thickness and support spacing but also support gap [37]. On the other hand, line support with 0.76 mm support thickness and 1.02 mm support spacing is the worst parameter set for the highest average thickness deviation.

ANOVA results for average thickness deviation are shown in Table 4. In this table, DF is the degree of freedom of the investigated parameter, Adj MS (adjusted mean squares) measures the variation of investigated parameter, Adj SS (adjusted sum of squares) measures the variations, F is a value used to calculate p value which is used to evaluate the significance of the investigated parameter on the design output [38].

According to the ANOVA results in Table 4, it can be concluded that support type is the most influential ($p = 0.0003 < 0.05$) and support thickness is the least influential ($p = 0.2237 > 0.05$) parameter on average thickness deviation.

Color-mapped surface deviations of upskin and downskin faces of three specimens related with three different support types are shown in Fig. 12. A detailed look in Fig. 12 can reveal that there is higher surface deviation and distortions on downskin surfaces than upskin surfaces for specimens supported by contactless supports (specimens 1–9). However, for specimens supported by line supports (specimens 10–18) and tooth supports (specimens 19–27), the situation is the opposite: higher surface deviation and distortions were observed on upskin surfaces. This can be attributed to the fact that, for line and tooth supports, the downskin surfaces are solidly supported and this results in lower distortions in downskin surfaces when compared to the upskin surfaces which are freestanding. On the other hand, for contactless supports, since there is no direct connection between the downskin surface and the supports, melt pool penetrates towards the powder bed during manufacturing and this phenomenon increases the distortions on downskin surfaces, however, upskin surfaces are supported by the previous molten and solidified layers to some extent which reduces the distortions on upskin surfaces. It is clear from Fig. 12 that the distortion on the downskin surface is not homogenous. Since support structures with multiple pieces were used in the present study, the nonhomogeneous distortion on downskin surfaces can be attributed to the different thermal dissipation behavior of supported areas and unsupported areas between two support pieces. Moreover, nearly for all specimens, the distortion at the tip of the specimen is higher than the root of the specimen due to the fact that the tip of the specimens is more freestanding when compared to the root of the specimens which have anchorage to the base plate.

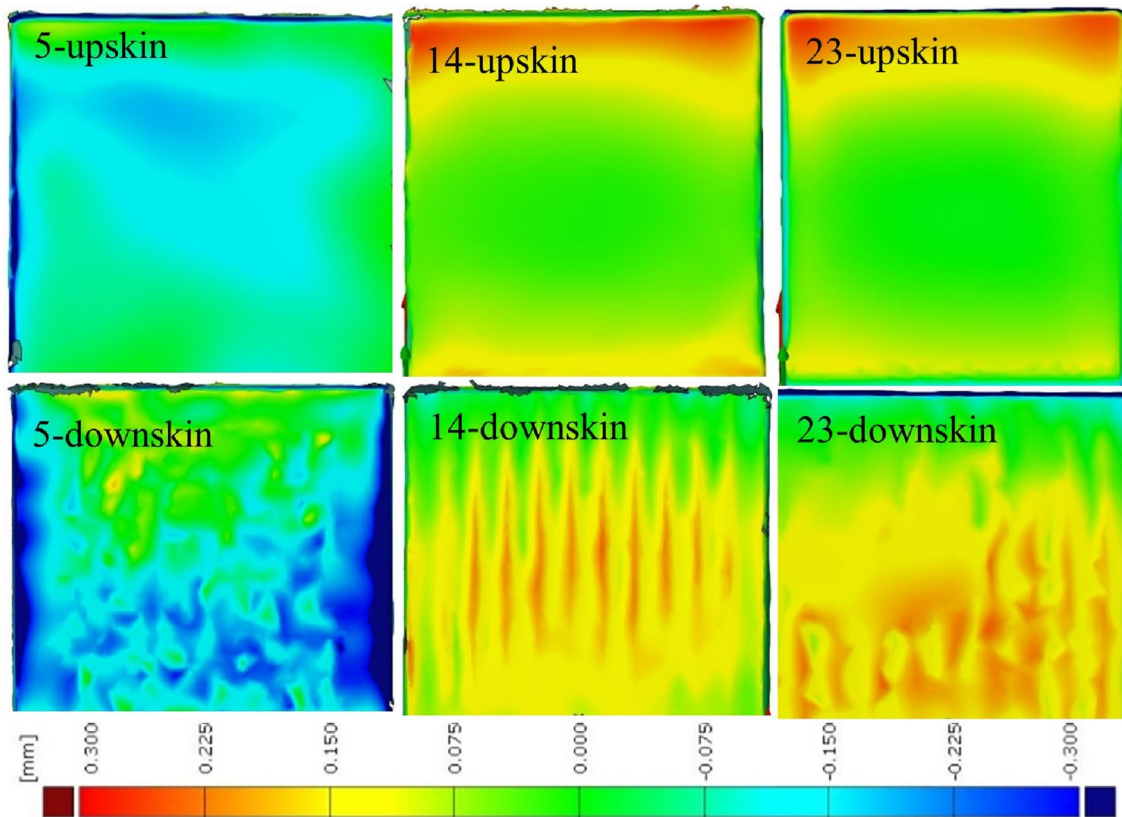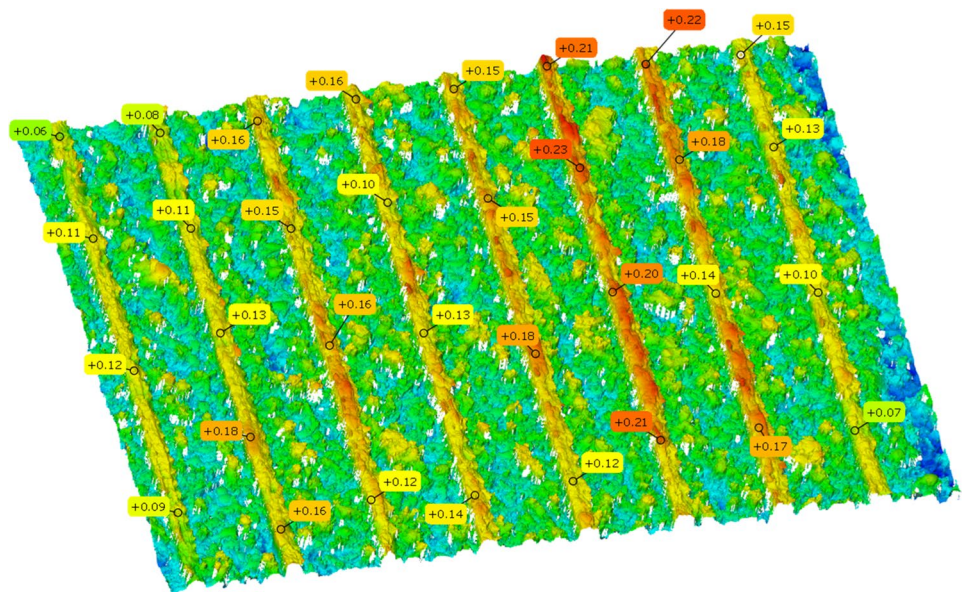For nearly all specimens supported by line and tooth supports, support remnants (Fig. 13) were observed on

Fig. 12 Color-mapped upskin and downskin surface deviations for three specimens related to three different support types. Numbers indicate specimen no

Fig. 13 Support remnant height measurements on surface texture map for a line supported specimen

downskin surfaces. It is clear from Fig. 12 that there are more support remnants in specimens supported by line supports than those supported by tooth supports. The height of these support remnants was measured on surface texture maps (Fig. 13) and average values was shown in Fig. 14 for line supports. It is clear that increasing

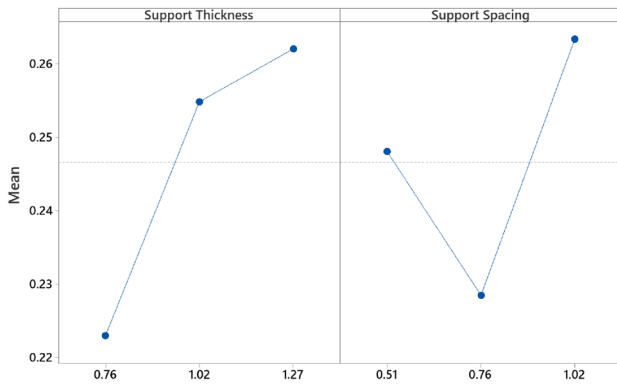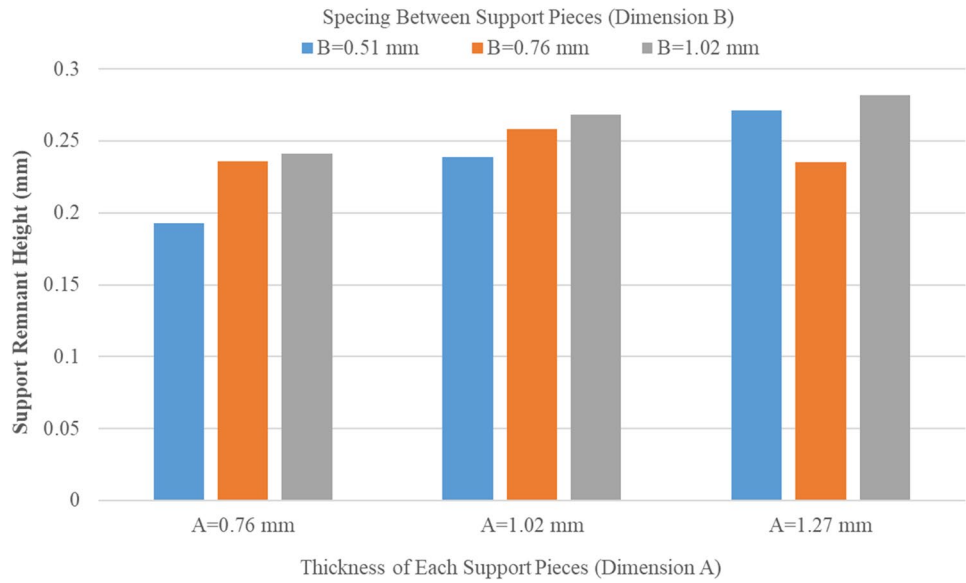**Fig. 14** Support remnant heights for line supported specimens

Fig. 15 Main effect plot for support remnant height

Table 5 ANOVA for support remnant height

Source	DF	Adj SS	Adj MS	*F* value	*p* value
Support thickness	2	0.002587	0.001293	4.42	0.097
Support spacing	2	0.001833	0.000916	3.13	0.152
Error	4	0.001171	0.000293		
Total	8				

support spacing and support thickness generally resulted in higher support remnants. This phenomenon is also clear from ANOVA analysis as shown in Fig. 15. The minimum and maximum support remnant heights were observed at 0.51 mm support spacing with 0.76 mm support thickness and at 1.02 mm support spacing with 1.27 mm support thickness, respectively.

ANOVA results for support remnant height of line-supported specimens are shown in Table 5. According to the ANOVA results, by comparing p values, it can be concluded

that support thickness has higher influence than support spacing on support remnant height.

3.2 Surface roughness results

Alicona measurements gave the whole surface topography or surface texture of the downskin surfaces. Surface roughness measurements were performed on surface texture maps extracted from Alicona by using GOM Inspect software. The measurements were performed on six different locations away from the supported areas where thickness deviation measurements were performed as shown in Fig. 9. Figure 16 shows the effect of support thickness and support spacing on surface roughness for contactless, line and tooth supports. For contactless supports, the minimum surface roughness (49.99 μm) was observed at 0.51 mm support spacing and 0.76 mm support thickness. On the other hand, the maximum surface roughness (70.82 μm) was observed at 1.02 mm support spacing and 0.76 mm support thickness. It can be generally stated that surface roughness increased with an increase in support spacing for fixed support thicknesses.

For line supports, the minimum surface roughness (44.71 μm) was observed at 0.51 mm support spacing and 0.76 mm support thickness. On the other hand, the maximum surface roughness (55.11 μm) was observed at 0.51 mm support spacing and 1.27 mm support thickness. Similar to the contactless supports, surface roughness increased with an increase in support spacing for fixed support thicknesses, except for the 1.27 mm thick supports.

For tooth supports, the minimum surface roughness (48.78 μm) was observed at 1.02 mm support spacing and 0.76 mm support thickness. On the other hand, the maximum surface roughness (54.47 μm) was observed at 1.02 mm support spacing and 1.27 mm support thickness.
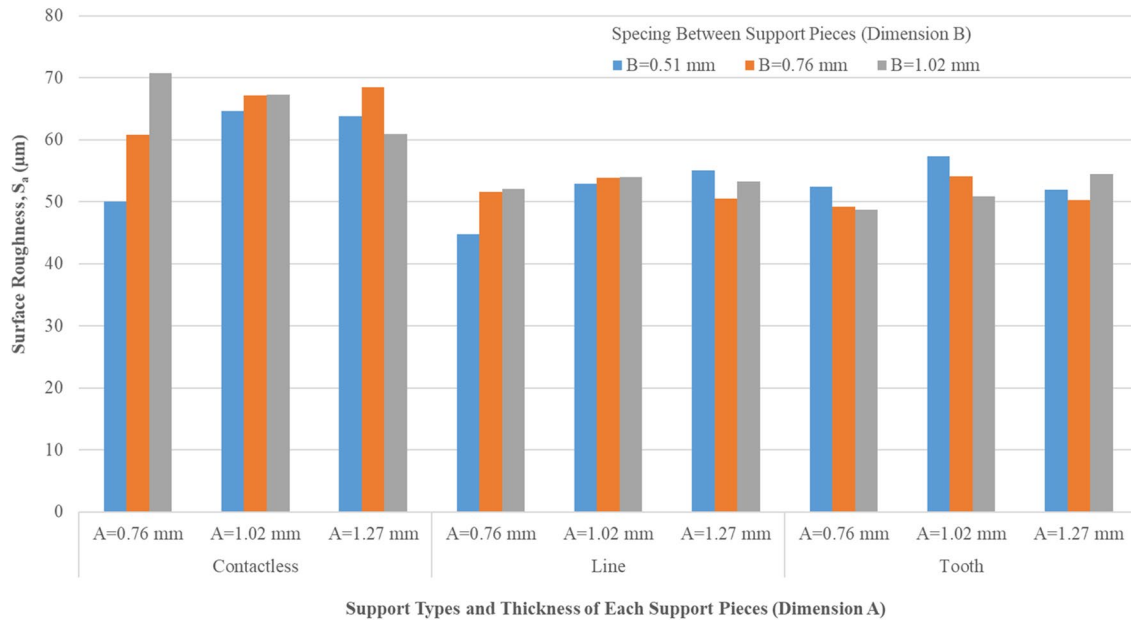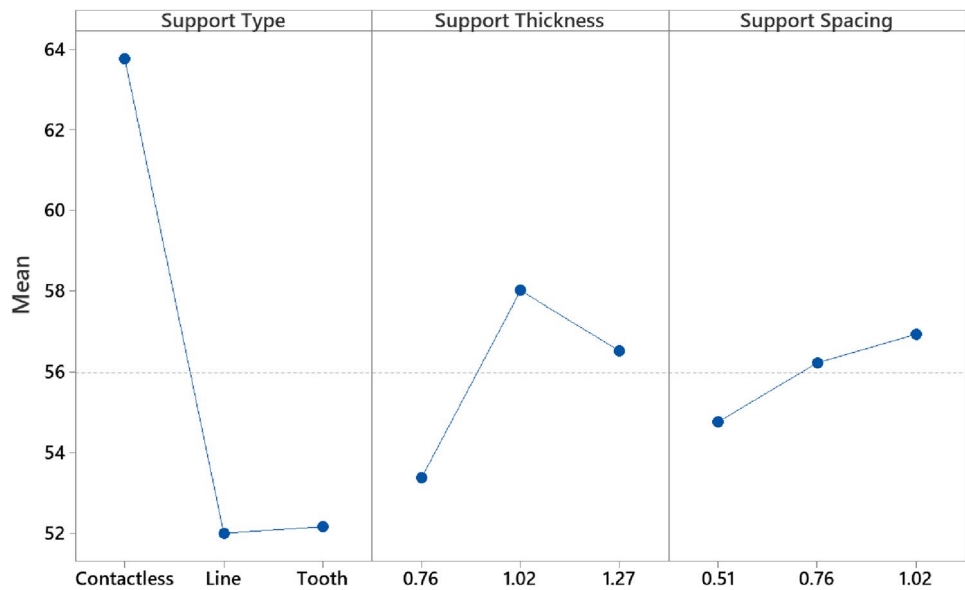
Fig. 16 Surface roughness values for all specimens

Fig. 17 Main effect plot for surface roughness

The main effect plot from ANOVA analysis of surface roughness is shown in Fig. 17. Lower surface roughness means higher performance, therefore, line support with 0.76 mm support thickness and 0.51 mm support spacing is the best parameter set for the lowest surface roughness and contactless support with 1.02 mm support thickness and 1.02 mm support spacing is the worst parameter set for the highest surface roughness.

From ANOVA results related to surface roughness (Table 6), support type is found to be the most influential and support spacing is the least influential ($p = 0.5096 > 0.05$) parameter. For contactless-type

Table 6 ANOVA for surface roughness

Source	DF	Adj SS	Adj MS	F value	p value
Support type	2	817.29	408.65	25.79	0.0000
Support thickness	2	100.48	50.24	3.17	0.0637
Support spacing	2	22.10	11.05	0.70	0.5096
Error	20	316.93	15.85		
Total	26				

supports, it was also found in the literature that support spacing has a negligible effect on surface roughness [39].

Surface texture maps for three specimens related to three different support types are shown in Fig. 18. Since any rough surface consists of peaks and valleys, these are shown in different colors in surface texture maps. In Fig. 18, red, yellow and green-yellow colors represent peaks and blue and blue-green colors represent valleys. A comparative investigation of Figs. 16 and 18 shows that the fraction of peaks and valleys in surface texture maps is consistent with the surface roughness results. For instance, contactless supports resulted in higher surface roughness values compared with line and tooth supports. It is clear that specimens 1–9 (contactless supports) have higher red areas than specimens 10–18 (line supports) and specimens

19–27 (tooth supports). Support remnants can be clearly seen in especially line supports.

Alicona measurement is a line-of-sight dependent technique which means that if a rough surface is to be scanned, some data loss may be observed [40]. For this reason, along with Alicona measurements, it is more realistic to use cross-sectional optical microscope images for surface roughness characterization. Figure 19 shows the optical microscope images of downskin surfaces for three specimens related to three different support types in which different surface irregularities on the surface were observed. In LPBF, some surface irregularities can be observed due to material filling defects, localized lack of fusion, particles ejection from the melt pool, etc. and these defects change the surface morphology and surface roughness of the specimens [41].
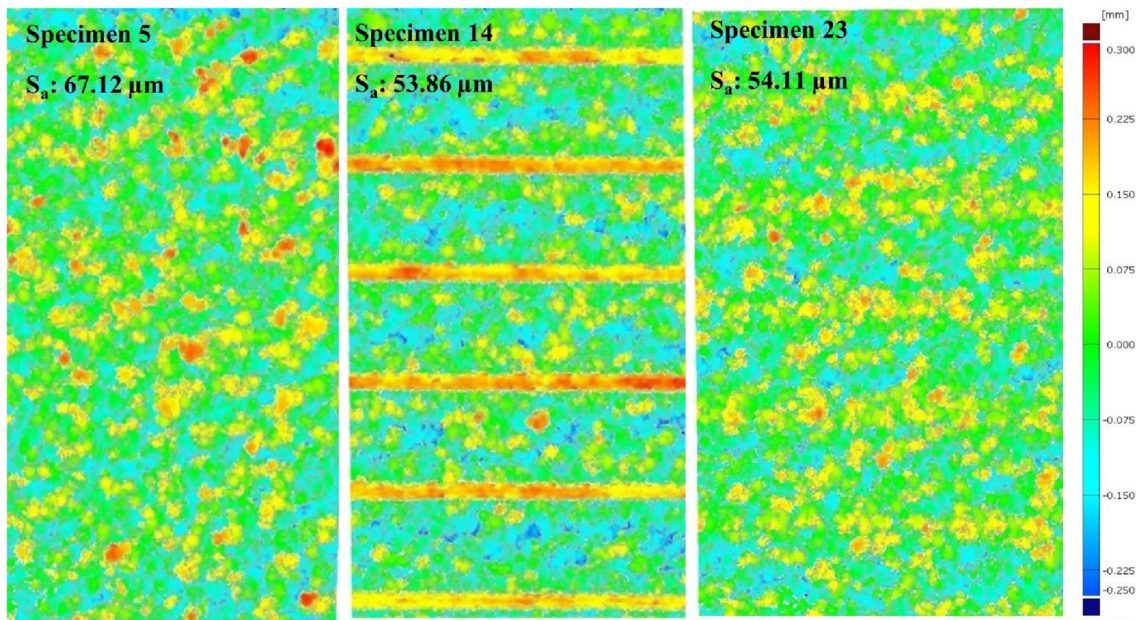

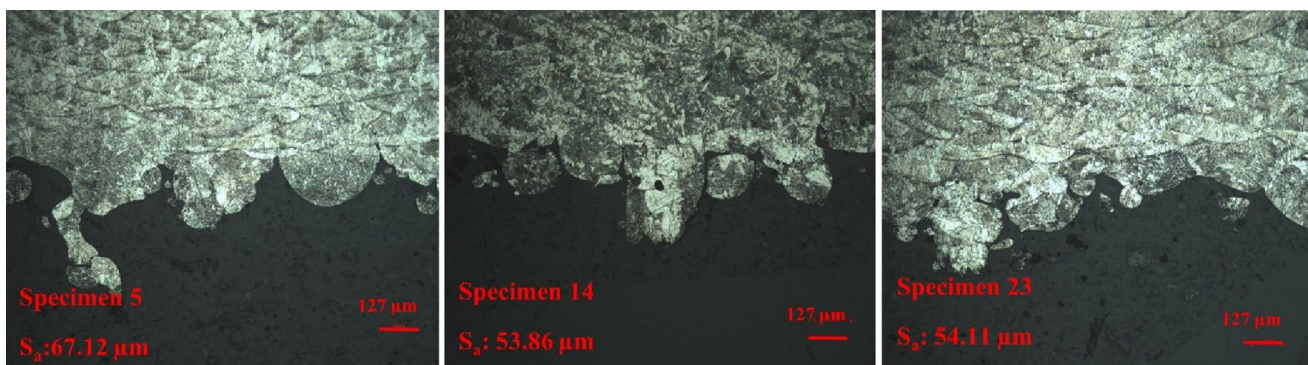**Fig. 18** Surface texture maps for three specimens related to three different support types

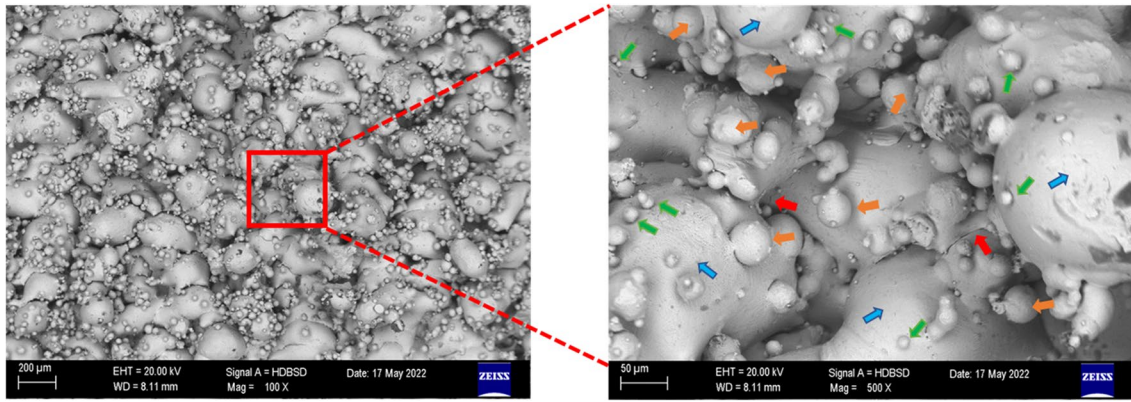**Fig. 19** Optical microscope images for three specimens related to three different support types

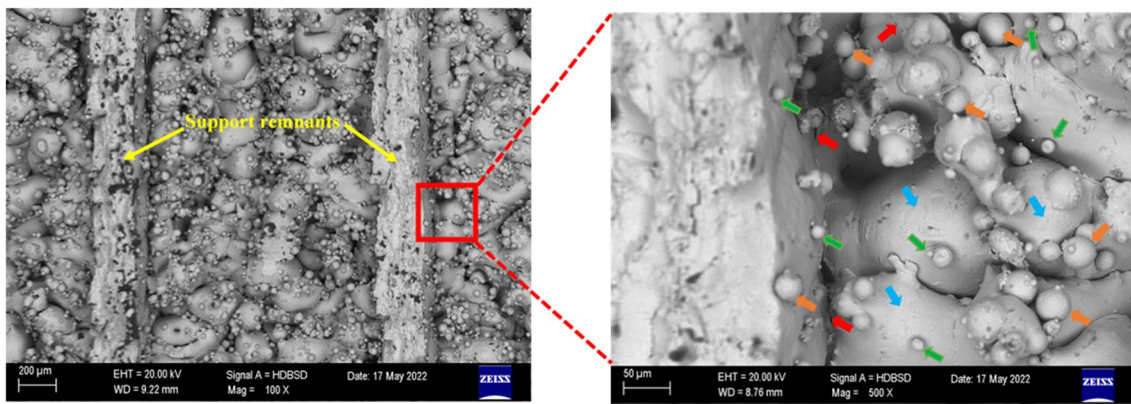**Fig. 20** SEM image of downskin surface of specimen 2 (contactless support)

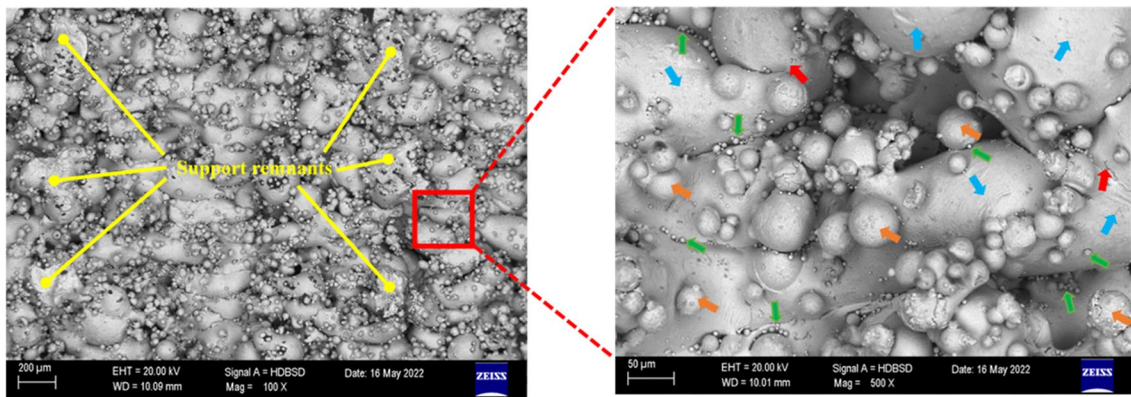**Fig. 21** SEM image of downskin surface of specimen 11 (line support)

Fig. 22 SEM image of downskin surface of specimen 25 (tooth support)

Figures 20, 21 and 22 show SEM images of downskin surfaces of specimens produced with contactless, line and tooth support, respectively. In all of the produced specimens, the phenomenon of attaching of non-fully melted powder particles to the surface due to lack of fusion [6] was observed as represented by green arrows in Figs. 20, 21, 22. In LPBF process, spattering is an unavoidable phenomenon due to the solidification and deposition of molten material ejected from the melt pool [42]. Due to the vapor pressure on the melt pool and entrapping laser energy, melted fluid in

the melt pool accelerates backwards. Spatters are formed at these locations [43]. Spattering powders can fall back onto the powder bed deteriorating the surface smoothness and may cause defects locally or can fall onto the consolidated surface which may fuse with it and may not be removed from the surface by the recoater blade [44]. After scanning of powders with laser energy, completely and non-fully melted powder particles may combine in large drops called balling phenomenon [45–47] and drops related to this phenomenon are shown in Figs. 20, 21, 22 with orange arrows. In Figs. 20, 21, 22, there are also bump or mushroom-like structures represented by blue arrows which are formed due to the expansion of the melt pool caused by the increase in viscosity. These structures are one of the main causes of surface roughness. Red arrows are shown in Figs. 20, 21, 22 which represent micro cracks. These cracks can penetrate very quickly and result in severe part failures [12]. Apart from these surface irregularities and micro cracks, remnants due to line and tooth supports are clearly visible in Fig. 21 and 22, respectively.

3.3 Microhardness results

Figure 23 shows the average microhardness measurements through the thickness of the specimens based on measurements at three locations: near the upper face, at the middle, and near the downskin face for three different support types. In reference [48], similar average microhardness results were also observed. For the contactless support

type, the minimum average microhardness (306.33 HV) was observed at 1.02 mm support spacing and 1.02 mm support thickness. On the other hand, the maximum average microhardness (313.67 HV) was observed at 0.51 mm support spacing and 1.02 mm support thickness. For line supports, the minimum average microhardness (303.67 HV) was observed at 0.76 mm support spacing and 1.27 mm support thickness. On the other hand, the maximum average microhardness (317.33 HV) was observed at 1.02 mm support spacing and 0.76 mm support thickness. In terms of tooth support used specimens, the minimum average microhardness (302.05 HV) was observed at 1.02 mm support spacing and 1.27 mm support thickness, whereas the maximum average microhardness (317.67 HV) was observed at 0.51 mm support spacing and 1.02 mm support thickness.

The main effect plot from ANOVA analysis is shown in Fig. 24. Higher or lower microhardness values can be desired in different applications. Therefore, it can be concluded that tooth support with 1.27 mm support thickness and 1.02 mm support spacing is the parameter set for the lowest amount of microhardness. On the other hand, line support with 0.76 mm support thickness and 0.51 mm support spacing is the parameter set for the highest amount of microhardness.

From ANOVA results related to surface roughness (Table 7), support spacing is found to be the most influential ($p = 0.0308 < 0.05$) and support type is the least influential ($p = 0.9057 > 0.05$) parameter.
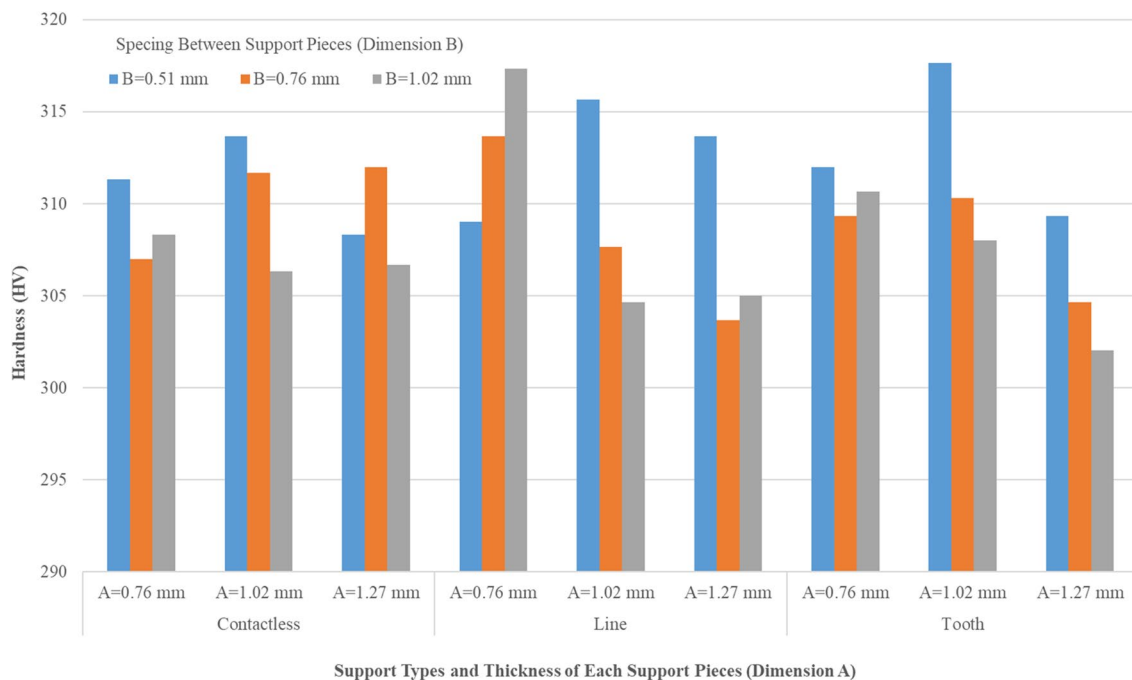

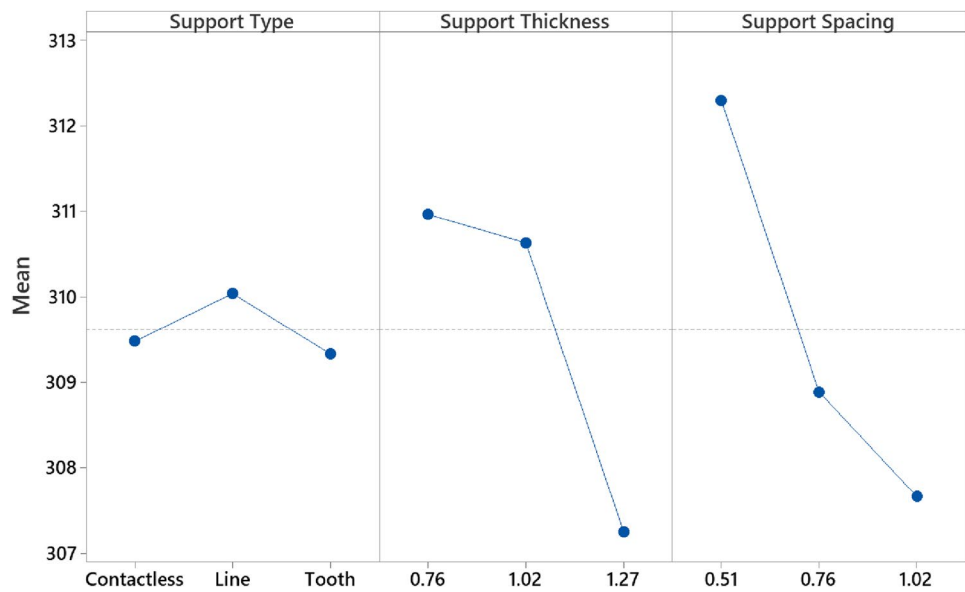**Fig. 23** Microhardness values for all specimens

Fig. 24 Main effect plot for microhardness

Table 7 ANOVA for microhardness

Source	DF	Adj SS	Adj MS	F value	p value
Support type	2	2.477	1.239	0.10	0.9057
Support thickness	2	75.564	37.782	3.04	0.0706
Support spacing	2	103.613	51.807	4.16	0.0308
Error	20	248.947	12.447		
Total	26				

Microhardness measurements at three different locations along with microstructure for three specimens related to three differ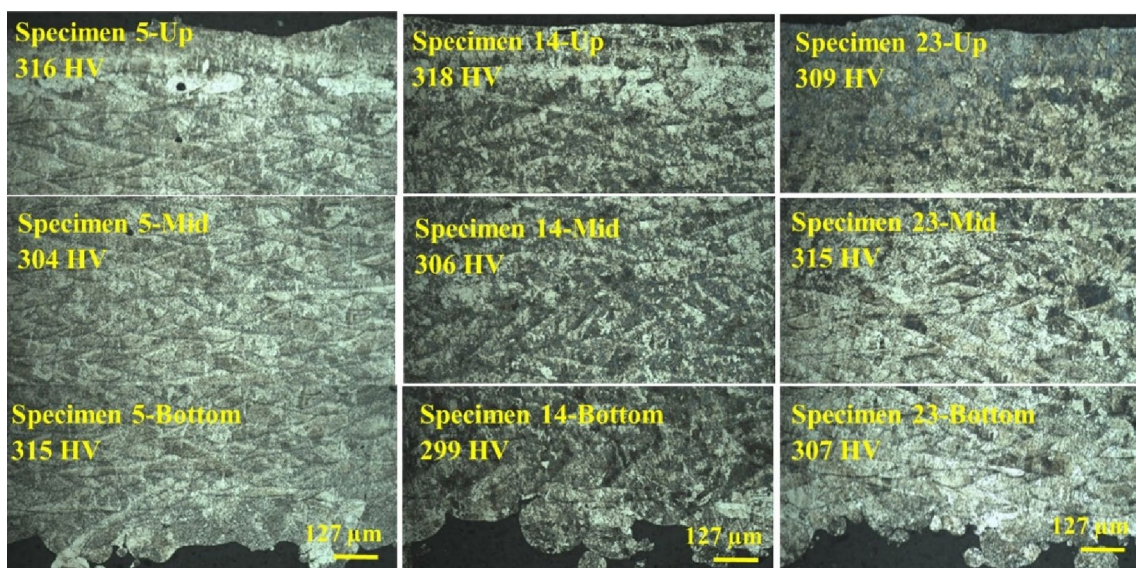ent support types is shown in Fig. 25. It is clear that microhardness increases from the top of the specimen to the bottom downskin surface for the specimens supported by contactless supports. However, this behavior is not obvious in specimens supported by line or tooth supports. Microhardness is directly related with the microstructure of the specimen. In specimens 1–9 where contactless supports are used, finer grains were observed at the near edge of the downskin surface and grains become coarser towards the upskin surface. At the downskin surface of the specimens, since the powder bed underneath is cold at the beginning of laser scanning and scanned powders are hot, large thermal gradients occur and because of high cooling rates, fine grains are formed. [49]. At higher build heights, since the

Fig. 25 Microhardness measurements at three different locations for three specimens related to three different support types

thermal difference between successive layers become low, coarser grains are formed [50]. A closer look into the optical images reveals that some fused particles were observed on the downskin surfaces. This phenomenon is observed for all types of support structures (Figs. 26, 27, 28). At the interface regions between fused particles and the specimens, columnar grains are observed which penetrate toward the inside of the specimen. These columnar grains are formed during the solidification of the scanned layers and have a direct effect on microhardness [51]. There are also some inner porosities

observed in Figs. 26, 27, 28 which decrease the mechanical behavior of the specimen.

4 Conclusion

In the present study, three different segmented support types, namely contactless support, line support and tooth support, are investigated in terms of dimensional deviation and distortion, surface roughness, microhardness through
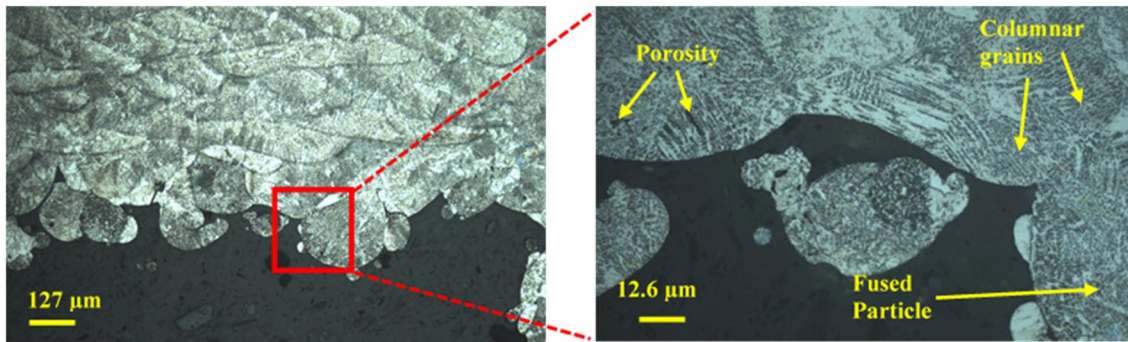

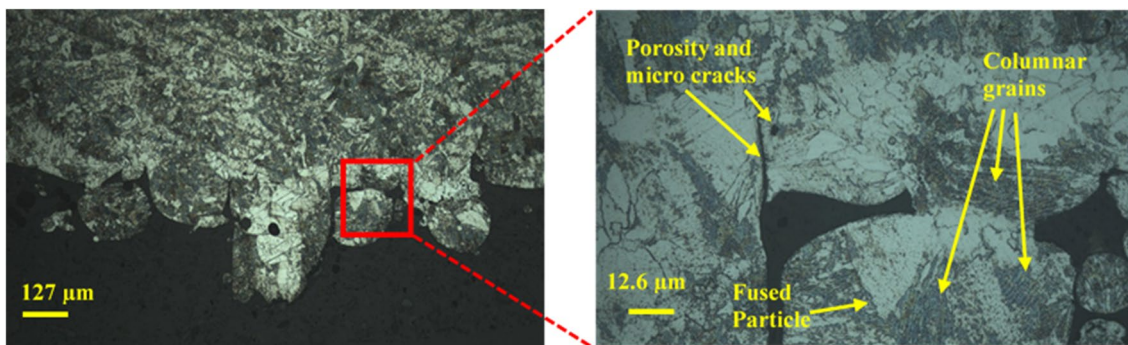**Fig. 26** Optical microscope image for specimen 3 (contactless support)

Fig. 27 Optical microscope image for specimen 14 (line support)
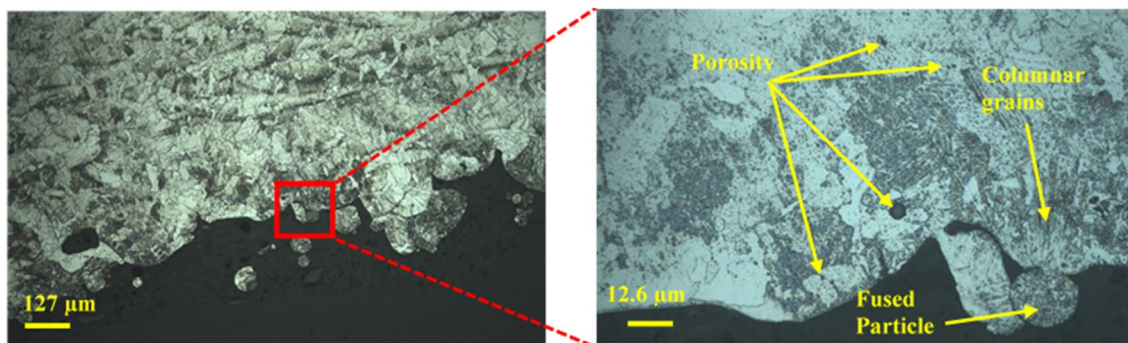

Fig. 28 Optical microscope image for specimen 24 (tooth support)

thickness and microstructure. Some key findings based on the experimental results are summarized as follows:

- Due to more freestanding melt pool penetration towards the loose powder bed, higher average thickness deviation occurs at higher support spacings for fixed support thickness in all types of supports. This behavior is more critical at thinner support segments. The minimum and maximum average thickness deviation were observed at the lowest and the highest support spacings, respectively.
- For contactless support type, an increase in segmented support thickness resulted in an increase in average thickness deviation.
- In contactless supports, higher surface deviation and distortions were observed on downskin surfaces than upskin surfaces. On the other hand, the opposite behavior was observed in specimens supported by line supports and tooth supports.
- Due to segmented support usage and resulting different thermal dissipation behavior of segmented sections and sections between two segments, complex deviations and distortions behavior were observed on downskin surfaces.
- Higher distortions were observed at the tip of the specimen compared with the root of the specimen for all types of supports due to free edge behavior.
- More support remnants were observed in line-supported specimens than tooth-supported specimens and remnant heights increased due to an increase in support spacing or support thickness.
- For contactless and line supports, higher support spacing resulted in higher surface roughness values.
- For all the specimens supported by different support types, some surface irregularities were observed which increase surface roughness and dimensional variations. These are: fused particles attached to the downskin surface, spattered powders from the melt pool and bump or mushroom-like structures on the surface.
- For contactless support types, microhardness at the lower edge is higher than microhardness at the upper edge due to microstructural changes. At lower edges, finer grains were observed.
- Using proper support thickness and spacing values, lower surface roughness and higher microhardness values can be achieved with line support. On the other hand, it results in higher thickness deviation than tooth and contactless support. Among the investigated support types, contactless support is the best option for the lowest average thickness deviation.
- Support type is found to be the most influential parameter on average thickness deviation and surface roughness.

In this study, overhang specimens were produced by the LPBF process from Inconel 718 powder material. Since different materials show different heating / cooling rates and thermal gradients, the findings in this article may not be applicable to other materials. Future studies will focus on the effectivity of using different types of support structures from different materials.

Data availability Data sets generated during the current study are available from the corresponding author on reasonable request.

Declarations

Conflict of interest The authors declare no conflict of interest. The funders had no role in the design of the study; in the collection, analyses, or interpretation of data; in the writing of the manuscript, or in the decision to publish the results. The authors have no competing interests to declare that are relevant to the content of this article.

References

1. Zhong RY, Xu X, Klotz E, Newman ST (2017) Intelligent manufacturing in the context of industry 4.0: a review. Engineering 3(5):616–630. https://doi.org/10.1016/J.ENG.2017.05.015
2. Avila JD, Bose S, Bandyopadhyay A (2018) Additive manufacturing of titanium and titanium alloys for biomedical applications. In: Froes FH, Qian M (eds) Titanium in medical and dental applications. Woodhead Publishing Series in Biomaterials, pp 325–343
3. Herzog D, Seyda V, Wycisk E, Emmelmann C (2016) Additive manufacturing of metals. Acta Mater 117:371–392. https://doi.org/10.1016/j.actamat.2016.07.019
4. Flores I, Kretzschmar N, Azman AH, Chekurov S, Pedersen DB, Chaudhuri A (2020) Implications of lattice structures on economics and productivity of metal powder bed fusion. Addit Manuf 31:100947. https://doi.org/10.1016/j.addma.2019.100947
5. Zakrzewski T, Kozak J, Witt M, Dębowska-Wąsak M (2020) Dimensional analysis of the effect of SLM parameters on surface roughness and material density. Procedia CIRP 95:115–120. https://doi.org/10.1016/j.procir.2020.01.182
6. Xiao Z, Yang Y, Xiao R, Bai Y, Song C, Wang D (2018) Evaluation of topology optimized lattice structures manufactured via selective laser melting. Mater Des 143:27–37. https://doi.org/10.1016/j.matdes.2018.01.023
7. Ma Z, Zhang DZ, Liu F, Jiang J, Zhao M, Zhang T (2018) Lattice structures of Cu–Cr–Zr copper alloy by selective laser melting: Microstructures, mechanical properties and energy absorption. Mater Des 187:108406
8. Charles A, Elkaseer A, Thijs L, Hagenmeyer V, Scholz S (2019) Effect of process parameters on the generated surface roughness of

down-facing surfaces in selective laser melting. Appl Sci 9:1256. https://doi.org/10.3390/app9061256

9. Maamoun AH, Xue YF, Elbestawi MA, Veldhuis SC (2018) Effect of selective laser melting process parameters on the quality of al alloy parts: powder characterization, density, surface roughness, and dimensional accuracy. Materials 11:2343. https://doi.org/10.3390/ma11122343

10. Pehlivan E, Roudnicka M, Dzugan J, Koukolikova M, Králík V, Seifi M, Lewandowski JJ, Dalibor D, Daniel M (2020) Effects of build orientation and sample geometry on the mechanical response of miniature CP-Ti Grade 2 strut samples manufactured by laser powder bed fusion. Addit Manuf 35:101403. https://doi.org/10.1016/j.addma.2020.101403

11. Leon A, Aghion E (2017) Effect of surface roughness on corrosion fatigue performance of AlSi10Mg alloy produced by selective laser melting (SLM). Mater Charact 131:188–194. https://doi.org/10.1016/j.matchar.2017.06.029

12. Ren D, Li S, Wang H, Hou W, Hao Y, Jin W, Yang R, Devesh R, Misra K, Murr LE (2019) Fatigue behavior of Ti-6Al-4V cellular structures fabricated by additive manufacturing technique. J Mater Sci Technol 35:285–294. https://doi.org/10.1016/j.jmst.2018.09.066

13. Spierings AB, Starr TL, Wegener K (2013) Fatigue performance of additive manufactured metallic parts. Rapid Prototyp J 19:88–94. https://doi.org/10.1108/13552541311302932

14. Jamshidinia M, Wang L, Tong W, Ajlouni R, Kovacevic R (2015) Fatigue properties of a dental implant produced by electron beam melting (EBM). J Mater Process Technol 226:255–263. https://doi.org/10.1016/j.jmatprotec.2015.07.013

15. Vayssette B, Saintier N, Brugger C, El May M, Pessard E (2018) Surface roughness of Ti-6Al-4V parts obtained by SLM and EBM: effect on the high cycle fatigue life. Procedia Eng 213:89–97. https://doi.org/10.1016/j.proeng.2018.02.010

16. Vayssette B, Saintier N, Brugger C, El May M, Pessard E (2019) Numerical modelling of surface roughness effect on the fatigue behavior of Ti–6Al-4V obtained by additive manufacturing. Int J Fatigue 123:180–195. https://doi.org/10.1016/j.ijfatigue.2019.02.014

17. Alfaify A, Saleh M, Abdullah FM, Al-Ahmari AM (2020) Design for additive manufacturing: a systematic review. Sustainability 12:7936. https://doi.org/10.3390/su12197936

18. Zhang K, Fu G, Zhang P, Ma Z, Mao Z, Zhang DZ (2019) Study on the geometric design of supports for overhanging structures fabricated by selective laser melting. Materials 12:27. https://doi.org/10.3390/ma12010027

19. Leary M (2017) Surface roughness optimisation for selective laser melting (SLM): accommodating relevant and irrelevant surfaces. In: Brandt M (ed) Laser additive manufacturing. Woodhead Publishing, pp 99–118. https://doi.org/10.1016/B978-0-08-100433-3.00004-X

20. Emmelmann C, Herzog D, Kranz J (2017) Design for laser additive manufacturing. In: Brandt M (ed) laser additive manufacturing. Woodhead Publishing, pp 259–279. https://doi.org/10.1016/B978-0-08-100433-3.00010-5

21. Huang R, Dai N, Cheng X, Wang L (2020) Topology optimization of lattice support structures for heat conduction in selective laser melting. Int J Adv Manuf Technol 109:1841–1851. https://doi.org/10.1007/s00170-020-05741-9

22. Järvinen JP, Matilainen V, Li X, Piili H, Salminen A, Mäkelä I, Nyrhilä O (2014) Characterization of effect of support structures in laser additive manufacturing of stainless steel. Phys Procedia 56:72–81. https://doi.org/10.1016/j.phpro.2014.08.099

23. Umer U, Ameen W, Abidi MH, Moiduddin K, Alkhalefah H, Alkahtani M, Al-Ahmari A (2019) Modeling the effect of different support structures in electron beam melting of titanium alloy using finite element models. Metals 9:806. https://doi.org/10.3390/met9070806

24. Cooper K, Steele P, Cheng B, Chou K (2018) Contact-free support structures for part overhangs in powder-bed metal additive manufacturing. Inventions 3(1):2. https://doi.org/10.3390/inventions3010002

25. Cheng B, Chou YK (2017) Overhang support structure design for electron beam additive manufacturing. In: Proceedings of the ASME 2017 12th International Manufacturing Science and Engineering Conference, June 4–8, Los Angeles, CA, USA

26. Cheng B, Chou K (2020) A numerical investigation of support structure designs for overhangs in powder bed electron beam additive manufacturing. J Manuf Process 49:187–195. https://doi.org/10.1016/j.jmapro.2019.11.018

27. Poyraz Ö, Yasa E, Akbulut G, Orhangül A, Pilatin S (2015) Investigation of support structures for direct metal laser sintering (DMLS) of In625 Parts. In: Solid Freeform Fabrication Symposium, Austin, Texas, USA, pp. 560–574

28. Calignano F (2014) Design optimization of supports for overhanging structures in aluminum and titanium alloys by selective laser melting. Mater Des 64:203–213. https://doi.org/10.1016/j.matdes.2014.07.043

29. Ameen W, Al-Ahmari A, Mohammed MK (2019) Self-supporting overhang structures produced by additive manufacturing through electron beam melting. Int J Adv Manuf Technol 104:2215–2232. https://doi.org/10.1007/s00170-019-04007-3

30. Ameen W, Mohammed MK, Al-Ahmari A, Ahmed N, Mian SH (2020) Investigation of support structure parameters and their affects during additive manufacturing of Ti6Al4V alloy via electron beam melting. Proc Inst Mech Eng, Part L: J Mater Des Appl. https://doi.org/10.1177/1464420720981668

31. Kurzynowski T, Stopyra W, Gruber K, Ziółkowski G, Kuźnicka B, Chlebus E (2019) Effect of scanning and support strategies on relative density of SLM-ed H13 steel in relation to specimen size. Materials 12:239. https://doi.org/10.3390/ma12020239

32. Kouraytem N, Chanut RA, Watring DS, Loveless T, Varga J, Spear AD, Kingstedt OT (2020) Dynamic-loading behavior and anisotropic deformation of pre-and post-heat-treated In718 fabricated by laser powder bed fusion. Addit Manuf 33:101083. https://doi.org/10.1016/j.addma.2020.101083

33. Bartolomeu F, Dourado N, Pereira F, Alves N, Miranda G, Silva FS (2020) Additive manufactured porous biomaterials targeting orthopedic implants: A suitable combination of mechanical, physical and topological properties. Mater Sci Eng C 107:110342. https://doi.org/10.1016/j.msec.2019.110342

34. Bartolomeu F, Fonseca J, Peixinho N, Alves N, Gasik M, Silva FS, Miranda G (2019) Predicting the output dimensions, porosity and elastic modulus of additive manufactured biomaterial structures targeting orthopedic implants. J Mech Behav Biomed Mater 99:104–117. https://doi.org/10.1016/j.jmbbm.2019.07.023

35. Ran Q, Yang W, Hu Y, Shen X, Yu Y, Xiang Y, Cai K (2018) Osteogenesis of 3D printed porous Ti6Al4V implants with different pore sizes. J Mech Behav Biomed Mater 84:1–11. https://doi.org/10.1016/j.jmbbm.2018.04.010

36. Sing SL, Miao Y, Wiria FE, Yeong WY (2016) Manufacturability and mechanical testing considerations of metallic scaffolds fabricated using selective laser melting: a review. Biomed Sci Eng 2(11):18–24. https://doi.org/10.4081/bse.2016.11

37. Gülcan O, Günaydın K, Çelik A, Yasa E (2022) The effect of contactless support parameters on the mechanical properties of laser powder bed fusion produced overhang parts. Int J Adv Manuf Technol 122:3235–3253. https://doi.org/10.1007/s00170-022-10135-0

38. Gülcan O, Simsek U, Cokgunlu O, Özdemir M, Şendur P, Yapici GG (2022) Effect of build parameters on the compressive behavior of additive manufactured CoCrMo lattice parts based on

experimental design. Metals 12(7):1104. https://doi.org/10.3390/met12071104

39. Gülcan O, Günaydın K (2022) Reducing support material usage in laser powder bed fusion parts: segmented passive support design for sustainable aviation. Towards Sustainable Aviation Summit, 18–20 October, Toulouse, France

40. Newton L, Senin N, Gomez C, Danzl R, Helmli F, Blunt L, Leach R (2019) Areal topography measurement of metal additive surfaces using focus variation microscopy. Addit Manuf 25:365–389. https://doi.org/10.1016/j.addma.2018.11.013

41. Tonelli L, Fortunato A, Ceschini L (2020) CoCr alloy processed by selective laser melting (SLM): effect of laser energy density on microstructure, surface morphology, and hardness. J Manuf Proces 52:106–119. https://doi.org/10.1016/j.jmapro.2020.01.052

42. Anwar AB, Ibrahim IH, Pham Q-C (2019) Spatter transport by inert gas flow in selective laser melting: a simulation study. Powder Technol 352:103–116. https://doi.org/10.1016/j.powtec.2019.04.044

43. Gunenthiram V, Peyre P, Schneider M, Dal M, Coste F, Koutiri I, Fabbro R (2018) Experimental analysis of spatter generation and melt-pool behavior during the powder bed laser beam melting process. J Mater Process Technol 251:376–386. https://doi.org/10.1016/j.jmatprotec.2017.08.012

44. Schniedenharn M, Wiedemann F, Schleifenbaum JH (2018) Visualization of the shielding gas flow in SLM machines by space-resolved thermal anemometry. Rapid Prototyp J 24(8):1296–1304

45. Li R, Liu J, Shi Y, Wang L, Jiang W (2012) Balling behavior of stainless steel and nickel powder during selective laser melting process. Int J Adv Manuf Technol 59:1025–1035. https://doi.org/10.1007/s00170-011-3566-1

46. Boutaous M, Liu X, Siginer DA, Xin S (2021) Balling phenomenon in metallic laser based 3D printing process. Int J Therm Sci 167:107011. https://doi.org/10.1016/j.ijthermalsci.2021.107011

47. Dwivedi S, Dixit AR, Das AK (2022) Wetting behavior of selective laser melted (SLM) bio-medical grade stainless steel 316L. Mater Today: Proc 56(1):46–50. https://doi.org/10.1016/j.matpr.2021.12.046

48. Karabulut Y, Tascioglu E, Kaynak Y (2021) Heat treatment temperature-induced microstructure, microhardness and wear resistance of Inconel 718 produced by selective laser melting additive manufacturing. Optik 227:163907. https://doi.org/10.1016/j.ijleo.2019.163907

49. Seede R, Mostafa A, Brailovski V, Jahazi M, Medraj M (2018) Microstructural and microhardness evolution from homogenization and hot isostatic pressing on selective laser melted Inconel 718: structure, texture, and phases. J Manuf Mater Process 2(2):30. https://doi.org/10.3390/jmmp2020030

50. Zhang B, Wang P, Chew Y, Wen Y, Zhang M, Wang P, Bi G, Wei J (2020) Mechanical properties and microstructure evolution of selective laser melting Inconel 718 along building direction and sectional dimension. Mater Sci Eng: A 794:139941. https://doi.org/10.1016/j.msea.2020.139941

51. Qi M, Huang S, Ma Y, Youssef SS, Zhang R, Qiu J, Lei J, Yang R (2021) Columnar to equiaxed transition during β heat treatment in a near β alloy by laser additive manufacture. J Mater Res Technol 13:1159–1168. https://doi.org/10.1016/j.jmrt.2021.05.057